Carotid Plaque Morphology and Composition: Initial Comparison between 1.5- and 3.0-T Magnetic Field Strengths[1]

Hunter R. Underhill, MD
Vasily L. Yarnykh, PhD
Thomas S. Hatsukami, MD
Jinnan Wang, MS
Niranjan Balu, PhD
Cecil E. Hayes, PhD
Minako Oikawa, MD, PhD
Wei Yu, MD
Dongxiang Xu, PhD
Baocheng Chu, MD, PhD
Bradley T. Wyman, PhD
Nayak L. Polissar, PhD
Chun Yuan, PhD

Purpose: To prospectively compare the interpretation and quantification of carotid vessel wall morphology and plaque composition at 1.5-T with those at 3.0-T magnetic resonance (MR) imaging.

Materials and Methods: Twenty participants (mean age, 69.8 years [standard deviation] ± 10.5; 75% men) with 16%–79% carotid stenosis at duplex ultrasonography were imaged with 1.5-T and 3.0-T MR imaging units with bilateral four-element phased-array surface coils. This HIPAA-compliant study was approved by the institutional review board, and all participants gave written informed consent. Protocols designed for similar signal-to-noise ratios across platforms were implemented to acquire axial T1-weighted, T2-weighted, intermediate-weighted, time-of-flight, and contrast material–enhanced T1-weighted images. Lumen area, wall area, total vessel area, wall thickness, and presence or absence and area of plaque components were documented. Continuous variables from different field strengths were compared by using the intraclass correlation coefficient (ICC) and repeated measures analysis. The Cohen κ was used to evaluate agreement between 1.5 T and 3.0 T on compositional dichotomous variables.

Results: There was a strong level of agreement between field strengths for all morphologic variables, with ICCs ranging from 0.88 to 0.96. Agreement in the identification of presence or absence of plaque components was very good for calcification ($\kappa = 0.72$), lipid-rich necrotic core ($\kappa = 0.73$), and hemorrhage ($\kappa = 0.66$). However, the visualization of hemorrhage was greater at 1.5 T than at 3.0 T (14.7% vs 7.8%, $P < .001$). Calcifications measured significantly ($P = .03$) larger at 3.0 T, while lipid-rich necrotic cores without hemorrhage were similar between field strengths ($P = .9$).

Conclusion: At higher field strengths, the increased susceptibility of calcification and paramagnetic ferric iron in hemorrhage may alter quantification and/or detection. Nevertheless, imaging criteria at 1.5 T for carotid vessel wall interpretation are applicable at 3.0 T.

[1] From the Departments of Radiology (H.R.U., V.L.Y., J.W., N.B., C.E.H., M.O., W.Y., D.X., B.C., C.Y.) and Surgery (T.S.H.), University of Washington, 815 Mercer St, Box 358050, Seattle, WA 98109; Pfizer, Groton, Conn (B.T.W.); and Mountain-Whisper-Light Statistical Consulting, Seattle, Wash (N.L.P.). Received June 25, 2007; revision requested August 23; revision received October 11; accepted December 19; final version accepted January 31, 2008. Supported by Pfizer and the National Institutes of Health (R01 HL61851, P01 HL072262, R01 HL073401, T-32 HL07838). **Address correspondence to** C.Y. (e-mail: *cyuan@u.washington.edu*).

Because stroke is a leading cause of long-term disability and the third most common cause of mortality in the United States, the primary clinical objective of carotid wall imaging is to improve the identification of plaques that pose an increased risk of future thromboembolic events. Recent technologic advances have enabled substantial gains in advancing noninvasive magnetic resonance (MR) imaging toward achieving this goal. Developments in radiofrequency coil (1) and pulse sequence design (2,3) have resulted in high-spatial-resolution imaging at 1.5 T for the in vivo quantitative evaluation of carotid wall morphology (4,5) and plaque composition (6–11). These advances, coupled with the high reproducibility of MR imaging data (12,13), have permitted serial monitoring of atherosclerotic disease evolution (14,15) and the identification of intraplaque risk factors for accelerated progression (16).

To further extend the exploration of in vivo carotid plaque morphology and composition, improved spatial resolution and/or signal-to-noise ratio (SNR) is necessary. In a recent investigation in which black-blood MR imaging with multiple weighting techniques at 1.5 T and 3.0 T were compared (17), significant increases in carotid wall SNR and lumen/wall contrast-to-noise ratio (CNR) were observed at the higher field strength. Moreover, reductions in both the imaging time and the in-plane acquisition resolution (from 0.63 mm at 1.5 T to 0.42 mm at 3.0 T) were also demonstrated. However, the previous study (17) involved a small number of subjects and did not focus on the compositional features of the atherosclerotic plaque, which are of primary clinical interest for predicting plaque vulnerability and assessment of disease progression. Although the improvements in a carotid imaging protocol at 3.0 T are promising for further clinical applications, the gain will be limited if the criteria for image interpretation at 1.5 T are not applicable at 3.0 T. Thus, the purpose of our study was to prospectively compare the interpretation and quantification of carotid vessel wall morphology and plaque composition at 1.5-T with those at 3.0-T MR imaging.

Advances in Knowledge

- MR imaging criteria validated at 1.5 T for the interpretation and quantification of carotid atherosclerotic disease can be applied to 3.0-T images.
- At higher field strengths, the increased susceptibility of calcification and paramagnetic ferric iron in hemorrhage may alter quantification and/or detection.

Materials and Methods

The study was supported in part by a grant from Pfizer (Groton, Conn). All authors (H.R.U., V.L.Y., T.S.H., J.W., N.B., C.E.H., M.O., W.Y., D.X., B.C., N.L.P., and C.Y.) who were not employees of the company had control of the data and the information for publication.

Participant Group

From August 28, 2006, to December 14, 2006, 20 asymptomatic participants (mean age, 69.8 years ± 10.5 [standard deviation]; range, 50–86 years; 75% men) with 16%–79% carotid stenosis as determined with duplex ultrasonography (US) underwent high-spatial-resolution carotid MR imaging at both 1.5 T and 3.0 T. A sample size of 20 subjects with one artery per patient was selected on the basis of the results of a previously published method comparison study (18). At the initial examination, all participants provided answers to a standardized health questionnaire and had their height and weight recorded. Our Health Insurance Portability and Accountability Act–compliant study was approved by the institutional review board of the University of Washington prior to study initiation, and all participants gave their written informed consent.

Implication for Patient Care

- The increased signal-to-noise ratio and/or additional spatial resolution afforded by imaging at 3.0 T should be utilized to further the understanding of atherosclerotic disease in patients.

MR Imaging Protocol

All MR imaging examinations were performed with 1.5-T (Signa Horizon EchoSpeed, version 5.8; GE Healthcare, Milwaukee, Wis) and 3.0-T (Achieva; Philips Medical Systems, Best, the Netherlands) platforms by using bilateral four-element phased-array surface coils. The 1.5-T coil was manufactured by a vendor (Pathway MRI, Seattle, Wash), and the 3.0-T coil was assembled with the same circuit board and configuration of elements. Both coil arrays were constructed to be similar to a previously published design (1).

With both the 1.5-T and 3.0-T MR imaging units, a standardized protocol with multiple weighting techniques (19) for carotid MR imaging was used to obtain two-dimensional (2D) T1-weighted, intermediate-weighted, and T2-weighted black-blood images and to perform three-dimensional (3D) time-of-flight (TOF) bright-blood angiography. In addition, a contrast material–enhanced black-blood T1-weighted sequence was performed 5 minutes after intravenous infusion of 0.1 mmol gadodiamide (Omniscan; GE Healthcare) per kilogram of body weight at

Published online before print
10.1148/radiol.2482071114

Radiology 2008; 248:550–560

Abbreviations:
CNR = contrast-to-noise ratio
ICC = intraclass correlation coefficient
SNR = signal-to-noise ratio
3D = three-dimensional
TOF = time of flight
2D = two-dimensional

Author contributions:
Guarantors of integrity of entire study, H.R.U., V.L.Y., T.S.H., W.Y.; study concepts/study design or data acquisition or data analysis/interpretation, all authors; manuscript drafting or manuscript revision for important intellectual content, all authors; manuscript final version approval, all authors; literature research, H.R.U., V.L.Y., T.S.H.; clinical studies, V.L.Y., T.S.H., N.B., B.C.; experimental studies, H.R.U., V.L.Y., T.S.H., J.W., N.B., C.E.H., M.O., W.Y., D.X.; statistical analysis, H.R.U., T.S.H., N.B., W.Y., N.L.P.; and manuscript editing, H.R.U., V.L.Y., T.S.H., N.B., C.E.H., M.O., B.T.W., N.L.P.

Funding:
This work was supported by the National Institutes of Health (grants R01-HL61851, P01-HL072262, R01-HL073401, T-32-HI07838).

See Materials and Methods for pertinent disclosures.

Parameters for Carotid MR Imaging Protocols at 1.5 T and 3.0 T

Parameter	T1-weighted Imaging with or without Contrast Enhancement		Intermediate-weighted Imaging		T2-weighted Imaging		TOF Imaging	
	1.5 T	3.0 T	1.5 T	3.0 T	1.5 T	3.0 T	1.5 T	3.0 T
Acquisition mode	2D	2D	2D	2D	2D	2D	3D	3D
Acquisition sequence	Fast spin echo	Turbo spin echo	Fast spin echo	Turbo spin echo	Fast spin echo	Turbo spin echo	Spoiled gradient recovery	T1-weighted fast field echo
Blood suppression technique	Quadruple inversion recovery	Quadruple inversion recovery	Multisection double inversion recovery	Multisection double inversion recovery	Multisection double inversion recovery	Multisection double inversion recovery	Saturation—veins	Saturation—veins
Repetition time (msec)	800	800	3000	4000	3000	4000	23	20
Echo time (msec)	11.0	9.0	8.9	8.0	53.7	52.0	3.6	4.8
Echo train length	10	11	12	12	12	12	None	None
Excitation flip angle (degrees)	90	90	90	90	90	90	25	20
No. of signals acquired	2	1	2	1	2	1	2	1
No. of sections*	12	16	12	16	12	16	16 (32)	24 (48)
Section thickness (mm)*	2	2	2	2	2	2	2 (1)	2 (1)
Coverage (mm)	24	32	24	32	24	32	32	48
Imaging time (min)	7	4	4	2.5	4	2.5	3	1.5

Note.—Field of view was 160 × 120 mm, matrix was 256 × 192, and spatial resolution was 0.63 × 0.63 mm^2 for all protocols. The quadruple inversion-recovery and multisection double inversion-recovery blood suppression techniques are described in references 2 and 3, respectively.

* Numbers in parentheses correspond to interpolated number of sections or section thickness after zero-filled Fourier transform in the slab direction.

a rate of 2 mL/sec. All images were acquired in the transverse plane and were centered at the bifurcation of the more diseased artery, the index artery, as identified at duplex US. The protocol for 3.0-T imaging was constructed to provide identical spatial resolution and similar SNRs for each sequence as the 1.5-T protocol (Table 1). On the basis of an expected increase in SNR at 3.0 T (17), one signal was acquired instead of the two signals acquired at 1.5 T. To avoid unwanted T1 weighting, intermediate-weighted and T2-weighted images at 3.0 T were obtained with a longer repetition time, anticipating an up to 30% increase in T1 at 3.0 T versus that at 1.5 T (20,21). For T1-weighted and 3D TOF images, no repetition time adjustment was performed because a possible enhancement of T1 contrast at the higher field strength was expected to be beneficial for such images. Owing to the feasibility of reducing the imaging time at 3.0 T, the 3.0-T protocol was implemented with a larger anatomic coverage (Table 1), which also allowed us to avoid potential data losses caused by section misregistration. Because 1.5-T images always corresponded to a central portion of 3.0-T images, 1.5-T data were fully utilized in the subsequent analysis.

In both the 1.5-T and 3.0-T protocols, identical custom-programmed blood suppression pulse sequences

Demographic Data in 20 Patients

Parameter	Datum
Age (y)*	69.8 ± 10.5
Height (cm)*	173.6 ± 8.8
Weight (kg)*	81.1 ± 18.1
Male sex	75 (15/20)
White race	90 (18/20)
History of hypertension	70 (14/20)
History of diabetes	20 (4/20)
History of hypercholesterolemia	100 (20/20)
Active smoker	50 (10/20)
Current statin therapy	90 (18/20)

Note.—Unless otherwise specified, data are percentages, with numbers used to calculate the percentages in parentheses.

* Data are means ± standard deviations.

were used. The long-repetition-time images (intermediate- and T2-weighted) were acquired with a time-efficient multisection double inversion-recovery blood suppression technique (3), with inversion times adjusted for blood T1 at 1.5 T and 3.0 T, as described previously (17). Pre- and postcontrast T1-weighted black-blood images were acquired by using a quadruple inversion-recovery sequence (2) that provided T1-insensitive blood suppression. All black-blood images were obtained with spectral-selective fat suppression to improve delineation of the outer wall boundary. After acquisition, all images underwent zero-filled interpolation to an image size of 512 × 512 pixels.

Image Review

Prior to image review, axial images of the index artery obtained with all contrast weightings were matched between platforms on the basis of distance from the bifurcation. Subsequently, teams of two reviewers (H.R.U., M.O., B.C., and W.Y., all with more than 1.5 years of experience in vascular MR imaging) who were blinded to both field strength and the corresponding images and results with the other platform, interpreted each axial location through consensus opinion. Image quality was assessed by using a four-point scale on which a score of 1 indicated poor quality (arterial wall and lumen margins not identifiable); a score of 2, adequate quality (arterial wall was visible, but the compositional substructure was partially obscured); a score of 3, good quality (minimal motion or flow artifacts, vessel wall and lumen boundaries clearly defined); and a score of 4, excellent quality (no artifacts, wall architecture and plaque composition depicted in detail). For images with image quality scores of 2 or greater, image analysis software (CASCADE [22]) was used to draw the lumen and outer wall boundaries. Metrics of arterial morphology were recorded as lumen area, wall area, total vessel area, normalized wall index (wall area divided by total vessel area), and mean wall thickness. In addition, the presence or absence of calcification, lipid-rich necrotic core, and hemorrhage were determined by using previously published criteria for imaging with multiple weighting techniques (7,8,10). Area measurements of each component, when present, were also collected.

SNR and CNR Calculations

Signal intensity data from a circular 12.5-mm^2 region of interest were sampled by a single reviewer (H.R.U.) from the background noise in the corner of each image devoid of signal and artifact. The mean signal intensity and standard deviation of the background noise region of interest, along with wall and lumen mean signal intensity, were documented for SNR and CNR calculations. As previously detailed by Yarnykh et al (17), SNR was determined for all black-blood images by using the following equation: $\mathrm{SNR} = (S_m^2 - N_m^2)^{1/2}/(\sigma/0.695)$, where S_m is the signal magnitude, N_m is the noise magnitude, σ is the measured standard deviation of the noise, and 0.695 is the adjustment applied to σ for a four-array coil design (23). SNR was determined for both the

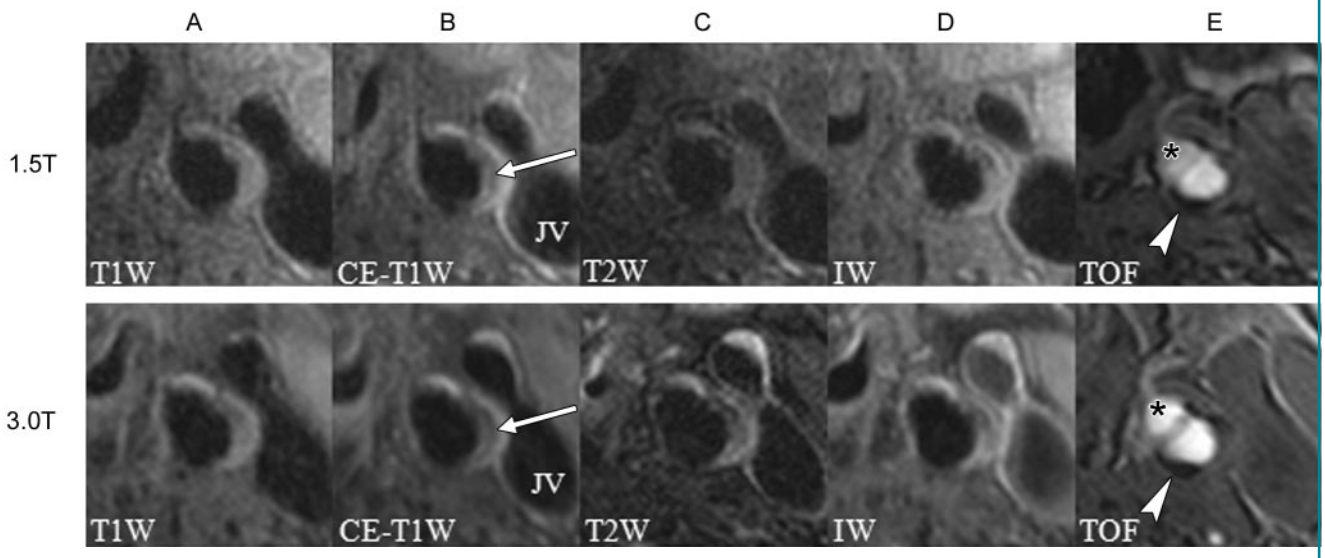

Figure 1: Matched axial cross-sectional images of left carotid bifurcation in 68-year-old man at 1.5 T (top) and 3.0 T (bottom). A lipid-rich necrotic core (column *B*, arrows) is apparent because of the decrease in signal intensity on the contrast-enhanced T1-weighted image *(CE-T1W)* compared with that on the precontrast T1-weighted *(T1W)* image and in surrounding fibrous tissue. The isointense signal on the TOF image in this region is consistent with an absence of hemorrhage at this location. Note the similarity in size of the lipid-rich necrotic core in the absence of hemorrhage. Other features of note: Superficial calcification (arrowheads, column *E*) is present with both platforms, and a branching vessel (∗ in column *E*), most likely the superior thyroid artery, is also present. *IW* = intermediate weighted, *JV* = jugular vein, *T2W* = T2 weighted.

Results of Comparison of Black-Blood Carotid MR Imaging SNRs and CNRs between 1.5-T and 3.0-T Imaging Units for 218 Matched Locations

Parameter, Field Strength, and Value	T1-weighted Imaging	T2-weighted Imaging	Intermediate-weighted Imaging	Contrast-enhanced T1-weighted Imaging
Wall SNR				
1.5 T*	15.7 ± 6.9	11.1 ± 5.2	20.6 ± 8.9	24.3 ± 10.8
3.0 T*	16.9 ± 8.0	14.1 ± 6.4	25.7 ± 13.2	24.9 ± 12.7
P value	.33	.001	.013	.57
Mean difference†	1.48 (−1.48, 4.44)	3.14 (1.20, 5.07)	5.03 (1.08, 8.99)	1.33 (−3.20, 5.85)
Lumen SNR				
1.5 T*	4.7 ± 2.5	3.6 ± 1.4	6.5 ± 3.3	7.5 ± 4.2
3.0 T*	4.5 ± 2.7	4.1 ± 2.9	8.5 ± 7.1	6.8 ± 4.4
P value	.79	.25	.11	.55
Mean difference†	−0.11 (−0.93, 0.71)	0.44 (−0.31, 1.18)	1.86 (−0.39, 4.11)	−0.46 (−1.97, 1.05)
CNR				
1.5 T*	11.0 ± 5.2	7.5 ± 3.2	14.1 ± 6.5	16.7 ± 7.9
3.0 T*	12.4 ± 6.4	10.0 ± 6.0	17.2 ± 8.9	18.2 ± 9.9
P value	.18	<.001	.002	.29
Mean difference†	1.43 (−0.65, 3.51)	2.67 (1.42, 3.92)	3.16 (1.18, 5.13)	1.62 (−1.37, 4.16)

* Data are means ± standard deviations.

† Value at 3.0 T minus that at 1.5 T. Data in parentheses are 95% confidence intervals.

Results of Comparison of Morphologic and Compositional Metrics at Matched Locations between 1.5-T and 3.0-T Imaging Units

Metric	No. of Matched Locations	Value at 1.5 T*	Value at 3.0 T*	*P* Value	Mean Difference†	ICC
Lumen area (mm^2)	218	26.4 ± 8.4	26.1 ± 7.9	.42	−0.32 (−1.11, 0.46)	0.96
Wall area (mm^2)	218	35.7 ± 8.7	36.1 ± 9.9	.60	0.28 (−0.77, 1.32)	0.91
Total vessel area (mm^2)	218	62.2 ± 13.0	62.2 ± 13.3	.90	−0.08 (−1.28, 1.12)	0.96
Normalized wall index	218	0.578 ± 0.133	0.585 ± 0.132	.20	0.006 (−0.003, 0.016)	0.91
Wall thickness (mm)	218	1.57 ± 0.34	1.59 ± 0.38	.43	0.02 (−0.03, 0.07)	0.88
Calcification (mm^2)	61	5.9 ± 6.2	7.9 ± 7.5	.03	1.60 (0.18, 3.02)	0.79
Lipid-rich necrotic core (mm^2)	50	14.9 ± 9.9	12.9 ± 10.8	.26	−1.39 (−3.83, 1.06)	0.83
Lipid-rich necrotic core without hemorrhage (mm^2)	21	9.3 ± 7.3	9.0 ± 8.4	.94	0.06 (−1.73, 1.85)	0.92
Hemorrhage (mm^2)	17	11.6 ± 8.7	8.7 ± 5.3	.17	−3.29 (−8.20, 1.61)	0.62

* Data are means ± standard deviations.

† Value at 3.0 T minus that at 1.5 T. Data in parentheses are 95% confidence intervals.

arterial wall and the lumen. Black-blood CNR was defined as the difference between wall and lumen SNRs.

Compositional Intensity

Intensity data for each plaque component (lipid-rich necrotic core, calcification, and intraplaque hemorrhage) and the fibrous tissue were collected (H.R.U., D.X.) from each matched axial location. The ratio of the component intensity to the intensity of fibrous tissue was calculated for T1-weighted, T2-weighted, intermediate-weighted, and TOF sequences for comparison between field strengths. Calculation of percentage contrast enhancement for lipid-rich necrotic core, calcification, intraplaque hemorrhage, and fibrous tissue was performed by using normalized signal intensities from the T1-weighted and contrast-enhanced T1-weighted sequences. Component intensity, including that of fibrous tissue, was normalized to that in the background noise region of interest at each axial location. Percentage contrast enhancement (%CE) for each component was subsequently determined by using the following equation: $\%CE = 100\% \cdot (S_{CE\text{-}T1W} - S_{T1W})/S_{T1W}$, where $S_{CE\text{-}T1W}$ is the normalized signal magnitude on contrast-enhanced T1-weighted images and S_{T1W} is the normalized signal magnitude on T1-weighted images.

Statistical Analysis

Repeated-measures analysis with either generalized estimating equations or lin-

ear mixed models was used when calculating the statistical significance and 95% confidence intervals of 3-T values minus 1.5-T values, at matched locations, compared with the null hypothesis value of zero (no difference). The repeated-measures method was used to accommodate the potential statistical dependence of multiple locations per artery. The generalized estimating equations method with a first-order autoregressive working correlation matrix was applied to comparisons between field strengths for SNR, CNR, image quality, and morphologic variables. Linear mixed models with a random intercept for the subject were used for continuous compositional variables because not all components were present in every artery.

The intraclass correlation coefficient (ICC) was used to describe the agreement in both morphologic and continuous compositional measurements between 1.5-T and 3.0-T modes, with the paired 1.5-T and 3.0-T values treated as repeated observations. The ICC considers the total variation in measurements across all of the arteries and calculates that proportion of the variation that cannot be attributed to method differences. ICCs close to 1.0 indicate good agreement between methods.

Visualization of lipid-rich necrotic core, calcification, and hemorrhage was calculated. Agreement between dichotomous compositional variables across all matched locations was assessed with the Cohen κ.

Analyses were performed by using software (SPSS for Windows, version 12.0, SPSS, Chicago, Ill; Stata, version 8.2, Stata, College Station, Tex; and the R statistical language, version 2.5.0, *http://www.r-project.org*). All data are reported as means ± standard deviations calculated across all locations for all arteries included in each analysis. $P < .05$ was considered to indicate a significant difference.

Results

Demographic data for the study group are presented in Table 2. Mean time between examinations at different field strengths was 22.4 days ± 20.6. From among the 20 index arteries imaged, there were 218 matched locations between the 1.5-T and 3.0-T imaging units available for analysis. The mean matched coverage per artery was 21.8 mm ± 1.9.

Image Quality, SNR, and CNR

No patient was excluded from analysis because of poor image quality. The mean observed image quality (Fig 1) was slightly improved at 3.0 T compared with that at 1.5 T (3.5 ± 0.6 vs 3.3 ± 0.6, $P < .08$). There was significant improvement in wall SNR and CNR for T2-weighted ($P = .001$ and $P < .001$, respectively) and intermediate-weighted ($P = .013$ and $P = .002$, respectively) images at 3.0 T. Wall SNR and CNR for T1-weighted and contrast-enhanced T1-weighted images did not change significantly (Table 3).

Morphology and Plaque Components

There was no significant difference in all measured morphologic variables between field strengths (Table 4). There was very good agreement in the identification of presence or absence of plaque components across all matched locations (Table 5), but hemorrhage was identified more often at 1.5 T than at 3.0 T. Of note, hemorrhage was identified at 15 more locations at 1.5 T than at 3.0 T and was never identified at 3.0 T when it was not present at 1.5 T (Fig 2).

For matched locations ($n = 61$) with the component variable present at both field strengths (Table 4), calcification was measured significantly ($P = .03$) larger at 3.0 T (Fig 2). Although there were trends present for a decrease in the size of hemorrhage ($n = 17$, $P = .17$) (Fig 3) and lipid-rich necrotic core ($n = 50$, $P = .26$) at 3.0 T, in the subset of lipid-rich necrotic cores without hemorrhage, there was no difference in necrotic core size between field strengths ($n = 21$, $P = .9$, Fig 1).

Relative intensity for each component compared with fibrous tissue was consistent between platforms, except for TOF imaging, which demonstrated a decrease at 3.0 T (Table 6). At both field strengths, lipid-rich necrotic core, calcification, and fibrous tissue demonstrated positive contrast enhancement (Table 6). The positive percentage contrast enhancement in hemorrhage was significant at neither 1.5 T ($P = .36$) nor 3.0 T ($P = .13$). At both field strengths, the lipid-rich necrotic core (Fig 1) and hemorrhage had less contrast enhancement than fibrous tissue (Table 6). Similarly, the contrast enhancement of calcification was less than that of fibrous tissue (Table 6).

Visualization of Compositional Features and Agreement between Platforms at 218 Matched Locations

Feature	1.5 T*	3.0 T*	Cohen κ
Lipid-rich necrotic core	30.3 (66/218)	26.7 (58/218)	0.73
Calcification	32.1 (79/218)	36.7 (80/218)	0.72
Hemorrhage	14.7 (32/218)	7.8 (17/218)	0.66

* Data are percentages, with numbers used to calculate the percentages in parentheses.

Discussion

There was strong agreement between 1.5 T and 3.0 T in quantitative measures of carotid plaque morphology (lumen area, wall area, total vessel area, normalized wall index, and mean wall thickness) and in the identification of plaque composition. Although there were differences in compositional area measurements, the findings presented herein support the translation of the histologically validated 1.5-T carotid MR image interpretation criteria to 3.0-T multisequence MR images.

Significant systematic differences in plaque morphologic measurements between GE and Philips MR imaging units at 1.5 T have recently been reported (18). Specifically, mean wall area and

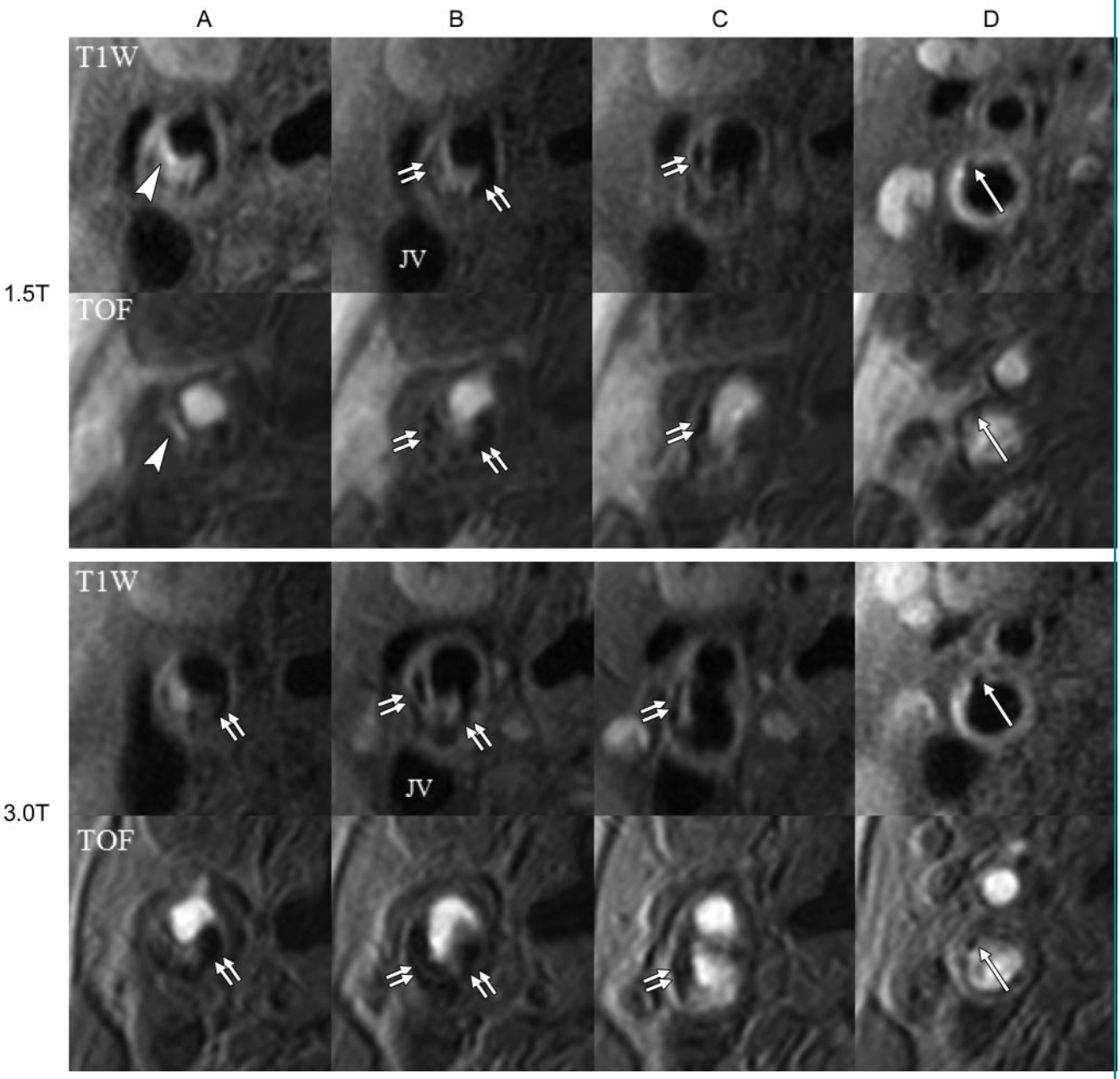

Figure 2: Serial matched locations of heavily calcified right carotid lesion at 1.5 T (top) and 3.0 T (bottom) in 82-year-old woman. In the common carotid artery (columns *A–C*), a large calcification (double arrows; hypointense signal on T1-weighted *[T1W]* and TOF images) is present. Observe the larger appearance of the calcification at 3.0 T, particularly on the TOF image. Additionally, note the extension of the calcification into the lumen (column *B*). In the internal carotid artery (column *D*), a small piece of calcification (single arrow) is present. The improved SNR at 3.0 T makes this piece appear larger and easier to detect with all contrast weightings. Of note, there is hyperintense signal (arrowhead) in column *A* on the T1-weighted and TOF 1.5-T images that is consistent with hemorrhage, but this signal is absent at 3.0 T. *JV* = jugular vein.

total vessel area were 12.4% and 4.7% larger with the GE imaging unit, while lumen area was 5.3% smaller with the GE unit than with the Philips unit. The identified difference in that study (18) was attributable to the employment of standard commercially available software and hardware unique to each platform type during image acquisition. For our investigation, customized pulse sequences (2,3) and protocols were designed to minimize these differences to

adequately isolate the effect of imaging at an increased field strength. In particular, the identical blood-suppression techniques multisection double inversion recovery and quadruple inversion recovery were utilized in both 1.5-T and 3.0-T imaging, and their timing parameters were appropriately adjusted. For the T1-weighted single-section imaging used for wall area measurements, the thickness of the reinverted section in the quadruple inversion-recovery preparative sequence was identical with both imaging units (4 mm). Subsequently, no systematic differences in quantitative plaque morphology were identified, and the ICCs were similar to previously reported data for interscan variability at 1.5 T for the same imaging unit type (13,24). As such, reported similarities and differences in plaque composition may be ascribed to differences in field strength rather than platform type.

Using the previously established criteria for identification of plaque components at 1.5 T, we found very good agreement between field strengths in the depiction of calcification, lipid-rich necrotic core, and hemorrhage across all matched locations. In addition, we found no differences in relative signal intensity for each component in all contrast weightings with the exception of TOF, which can be attributed to the absence of repetition time adjustment in the 3.0-T imaging protocol. Furthermore, the reported measures of percentage contrast enhancement are consistent with previously published data (25) and with the established imaging criteria for identifying the lipid-rich necrotic core (7). Of note, the percentage contrast enhancement results for calcification are most likely related to the increased effects of noise and subtle registration errors during data acquisition for small calcifications. We believe these collective findings provide compelling evidence that the tissue contrast criteria developed at 1.5 T for carotid plaque interpretation are applicable at 3.0 T. There were, however, apparent differences in the measured size of particular components.

The difference in area measurements of calcification may be attributable to a combination of increased susceptibility at the higher field strength and the improved SNR and perceived image quality at 3.0 T compared with those at 1.5 T during this investigation. The former would increase the apparent size of calcifications, while the latter would make it easier to detect smaller pieces of calcification. Comparisons of 1.5-T quantitative MR imaging results with histologic results (8) have shown that the size of calcification is underestimated at MR imaging. Moreover, the sensitivity for detection of calcification is decreased when the area at histologic examination is less than 2 mm^2. The identified effects of imaging at 3.0 T on calcification may not only improve sensitivity but may also provide a more accurate representation of in vivo plaque composition than was previously available at 1.5 T.

The trend toward a smaller measured lipid-rich necrotic core at 3.0 T was most likely an effect of hemorrhage identification. There was an increase in the detection frequency of hemorrhage and a trend toward larger measured areas of hemorrhage at 1.5 T. In postmortem studies of coronary atherosclerosis (26), intraplaque hemorrhage has been identified to occur within the necrotic core. In carotid vessel disease, the most

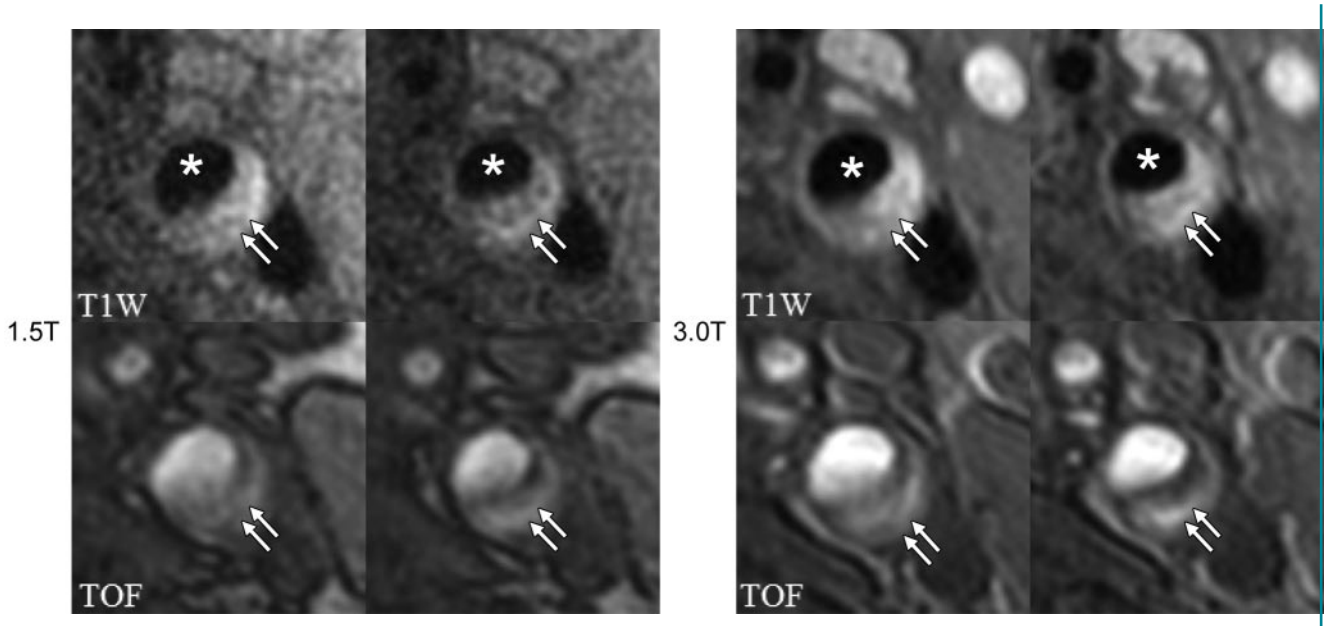

Figure 3: Comparison of advanced lesion in left internal carotid artery in 65-year-old man at 1.5 T (left) and 3.0 T (right). Intraplaque hemorrhage (arrows) is present in this lesion, identifiable by the hyperintense signal on T1-weighted *(T1W)* and TOF images at both field strengths. Of note, the image quality at 3.0 T is improved compared with that in matched locations at 1.5 T. * = Lumen of internal carotid artery.

common underlying lesion associated with hemorrhage is a lipid-rich atheroma with a necrotic core (11). Hence, boundaries for quantification of the lipid-rich necrotic core have been drawn to include intraplaque hemorrhage during previous MR imaging investigations (16,27). The increased visualization of hemorrhage at 1.5 T and the subsequent inclusion of hemorrhage within the identified boundary of the lipid-rich necrotic core most likely resulted in the area difference between field strengths. Moreover, in the absence of hemorrhage, there was no difference in the measurement of lipid-rich necrotic core between 1.5 T and 3.0 T.

The discrepancies in the detection and measurement of intraplaque hemorrhage can be attributed to inherent biophysical properties of the hemorrhage itself. As known from histologic studies (28), the hemorrhagic component of advanced atherosclerotic lesions contains blood degradation products of various ages. Such blood degradation products (eg, methemoglobin, hemosiderin, ferritin) contain paramagnetic ferric iron, which strongly increases magnetic susceptibility and correspondingly reduces MR signal. At higher field strengths, the more pronounced susceptibility effect may result in cancellation of the signal enhancement with T1-weighted sequences, which is the major imaging sign of an intraplaque hemorrhage (10). The decreased hemorrhage signal intensity at 3.0 T on T1-weighted and TOF images reported in our study supports this explanation. Similarly, the susceptibility effect of the deposited iron on the signal from brain tissues was shown to be more significant at 3.0 T than at 1.5 T (29). Although this can explain the difference in hemorrhage detection rates and measured areas, it also should be taken into account that this study employed the histologically validated imaging criteria established at 1.5 T, which have been reported to yield a high sensitivity but a relatively low specificity (74%) (10). An alternative explanation may assume an improvement in specificity at 3.0 T due to elimination of false-positive results as a result of overall improvement in image

Component Signal Intensity Relative to That of Fibrous Tissue and Percentage Contrast Enhancement for Each Component

Parameter, Imaging Type, and Value	1.5 T	3.0 T	*P* Value*	Mean Difference†
Lipid-rich necrotic core ($n = 50$)				
T1-weighted imaging	1.24 ± 0.17	1.21 ± 0.17	.12	−0.03 (−0.07, 0.01)
T2-weighted imaging	1.17 ± 0.17	1.16 ± 0.19	.67	−0.02 (−0.10, 0.07)
Intermediate-weighted imaging	1.11 ± 0.22	1.10 ± 0.23	.50	−0.02 (−0.09, 0.04)
TOF imaging	1.18 ± 0.43	1.04 ± 0.36	<.001	−0.14 (−0.22, −0.06)
Percentage contrast enhancement	24.2 ± 32.8	21.5 ± 36.8	.8‡	−2.65 (−21.3, 16.0)
P value for comparison of percentage contrast enhancement with zero	.02	.003	. . .	. . .
P value for comparison of percentage contrast enhancement with that of fibrous tissue	<.001	<.001	. . .	. . .
Calcification ($n = 61$)				
T1-weighted imaging	0.75 ± 0.22	0.72 ± 0.24	.60	−0.02 (−0.11, 0.06)
T2-weighted imaging	0.74 ± 0.21	0.72 ± 0.22	.90	−0.01 (−0.09, 0.08)
Intermediate-weighted imaging	0.65 ± 0.22	0.65 ± 0.25	.83	−0.01 (−0.11, 0.09)
TOF imaging	0.60 ± 0.21	0.51 ± 0.18	.012	−0.08 (−0.15, −0.02)
Percentage contrast enhancement	31.6 ± 52.8	32.8 ± 43.7	.9	1.10 (−16.5, 18.7)
P value for comparison of percentage contrast enhancement with zero	<.001	<.001	. . .	. . .
P value for comparison of percentage contrast enhancement with that of fibrous tissue	.3§	.02	. . .	. . .
Hemorrhage ($n = 17$)				
T1-weighted imaging	1.34 ± 0.23	1.08 ± 0.40	.02	−0.27 (−0.49, −0.04)
T2-weighted imaging	1.14 ± 0.23	0.99 ± 0.52	.38	−0.22 (−0.74, 0.30)
Intermediate-weighted imaging	0.98 ± 0.24	0.87 ± 0.38	.24	−0.15 (−0.41, 0.11)
TOF imaging	1.81 ± 0.57	1.46 ± 0.44	.003	−0.36 (−0.57, −0.14)
Percentage contrast enhancement	13.0 ± 26.9	20.5 ± 47.0	.9	3.31 (−47.1, 53.7)
P value for comparison of percentage contrast enhancement with zero	.4	.13	. . .	. . .
P value for comparison of percentage contrast enhancement with that of fibrous tissue	<.001	.007	. . .	. . .
Fibrous tissue ($n = 218$)				
Percentage contrast enhancement	41.7 ± 39.4	43.8 ± 37.1	.8	1.65 (−13.9, 17.2)
P value for comparison of percentage contrast enhancement with zero	<.001	<.001	. . .	. . .

Note.—Unless otherwise specified, data are means ± standard deviations.

* For comparison of value at 1.5 T with that at 3.0 T.

† Value at 3.0 T minus that at 1.5 T. Data in parentheses are 95% confidence intervals.

‡ $P = 0.2$ without an outlier.

§ $P = .009$ without an outlier.

quality. More research comparing MR imaging findings with a histologic reference standard is necessary to assess the accuracy of hemorrhage identification at 3.0 T. Possible improvement of hemorrhage detection at both field strengths may also be achieved with heavily T1-weighted sequences like those proposed by Moody et al (9).

Although the protocols used in our study were designed to provide similar SNRs, there was a slight improvement in SNR at 3.0 T. This is consistent with theoretic expectations, which predict an improvement in SNR due to the increased field strength, despite fewer excitations during image acquisition. An increase in SNR at 3.0 T in our study favorably compares with previous results (17), in which the factors of SNR increase for identical imaging protocols were in a range 1.5–1.8 for different contrast weightings. Our data are consistent with these factors scaled by the value of $\sqrt{2}$ as a result of acquiring one signal at 3.0 T instead of averaging two signals at 1.5 T.

There were several limitations to this study. First, the MR imaging units utilized in this investigation were from different manufacturers. Although the acquisition protocols were optimized to minimize differences between the imaging units, postprocessing features specific to each unit were not disabled. Second, there was a relatively low prevalence of hemorrhage within the evaluated population. Future investigations should not only include more hemorrhagic lesions but should also have histologic results available as the reference standard. Finally, the interval between examinations may have allowed the hemorrhage signal to change. Although previous investigations have demonstrated a consistent hemorrhage signal in carotid plaques even after an interval of 18 months (16), serial studies that directly evaluate the time course of intraplaque hemorrhage signal evolution are necessary at both field strengths.

We believe our study provides evidence for several conclusions. First, imaging criteria validated at 1.5 T for the interpretation and quantification of carotid atherosclerotic disease can be applied to 3.0-T imaging. Second, patients enrolled in serial prospective investigations should be imaged at the same field strength at all time points to minimize bias and interstudy error during compositional analysis. Finally, the increased SNR and/or additional spatial resolution afforded by imaging at 3.0 T should be exploited to further the understanding of in vivo atherosclerotic disease.

References

1. Hayes CE, Mathis CM, Yuan C. Surface coil phased arrays for high-resolution imaging of the carotid arteries. J Magn Reson Imaging 1996;6(1):109–112.
2. Yarnykh VL, Yuan C. T1-insensitive flow suppression using quadruple inversion-recovery. Magn Reson Med 2002;48(5):899–905.
3. Yarnykh VL, Yuan C. Multislice double inversion-recovery black-blood imaging with simultaneous slice reinversion. J Magn Reson Imaging 2003;17(4):478–483.
4. Yuan C, Beach KW, Smith LH Jr, Hatsukami TS. Measurement of atherosclerotic carotid plaque size in vivo using high resolution magnetic resonance imaging. Circulation 1998; 98(24):2666–2671.
5. Fayad ZA, Fuster V. Characterization of atherosclerotic plaques by magnetic resonance imaging. Ann N Y Acad Sci 2000;902:173–186.
6. Toussaint JF, LaMuraglia GM, Southern JF, Fuster V, Kantor HL. Magnetic resonance images lipid, fibrous, calcified, hemorrhagic, and thrombotic components of human atherosclerosis in vivo. Circulation 1996;94(5): 932–938.
7. Cai J, Hatsukami TS, Ferguson MS, et al. In vivo quantitative measurement of intact fibrous cap and lipid-rich necrotic core size in atherosclerotic carotid plaque: comparison of high-resolution, contrast-enhanced magnetic resonance imaging and histology. Circulation 2005;112(22):3437–3444.
8. Saam T, Ferguson MS, Yarnykh VL, et al. Quantitative evaluation of carotid plaque composition by in vivo MRI. Arterioscler Thromb Vasc Biol 2005;25(1):234–239.
9. Moody AR, Murphy RE, Morgan PS, et al. Characterization of complicated carotid plaque with magnetic resonance direct thrombus imaging in patients with cerebral ischemia. Circulation 2003;107(24):3047–3052.
10. Chu B, Kampschulte A, Ferguson MS, et al. Hemorrhage in the atherosclerotic carotid plaque: a high-resolution MRI study. Stroke 2004;35(5):1079–1084.
11. Kampschulte A, Ferguson MS, Kerwin WS, et al. Differentiation of intraplaque versus juxtaluminal hemorrhage/thrombus in advanced human carotid atherosclerotic lesions by in vivo magnetic resonance imaging. Circulation 2004;110(20):3239–3244.
12. Kang X, Polissar NL, Han C, Lin E, Yuan C. Analysis of the measurement precision of arterial lumen and wall areas using high-resolution MRI. Magn Reson Med 2000;44(6): 968–972.
13. Saam T, Kerwin WS, Chu B, et al. Sample size calculation for clinical trials using magnetic resonance imaging for the quantitative assessment of carotid atherosclerosis. J Cardiovasc Magn Reson 2005;7(5):799–808.
14. Corti R, Fuster V, Fayad ZA, et al. Effects of aggressive versus conventional lipid-lowering therapy by simvastatin on human atherosclerotic lesions: a prospective, randomized, double-blind trial with high-resolution magnetic resonance imaging. J Am Coll Cardiol 2005;46(1):106–112.
15. Saam T, Yuan C, Chu B, et al. Predictors of carotid atherosclerotic plaque progression as measured by noninvasive magnetic resonance imaging. Atherosclerosis 2007;194(2):e34–e42.
16. Takaya N, Yuan C, Chu B, et al. Presence of intraplaque hemorrhage stimulates progression of carotid atherosclerotic plaques: a high-resolution magnetic resonance imaging study. Circulation 2005;111(21):2768–2775.
17. Yarnykh VL, Terashima M, Hayes CE, et al. Multicontrast black-blood MRI of carotid arteries: comparison between 1.5 and 3 Tesla magnetic field strengths. J Magn Reson Imaging 2006;23(5):691–698.
18. Saam T, Hatsukami TS, Yarnykh VL, et al. Reader and platform reproducibility for quantitative assessment of carotid atherosclerotic plaque using 1.5T Siemens, Philips, and General Electric scanners. J Magn Reson Imaging 2007;26(2):344–352.
19. Yuan C, Mitsumori LM, Ferguson MS, et al. In vivo accuracy of multispectral magnetic resonance imaging for identifying lipid-rich necrotic cores and intraplaque hemorrhage in advanced human carotid plaques. Circulation 2001;104(17):2051–2056.
20. de Bazelaire CM, Duhamel GD, Rofsky NM, Alsop DC. MR imaging relaxation times of abdominal and pelvic tissues measured in vivo at 3.0 T: preliminary results. Radiology 2004;230(3):652–659.
21. Gold GE, Suh B, Sawyer-Glover A, Beaulieu C. Musculoskeletal MRI at 3.0 T: initial clini-

cal experience. AJR Am J Roentgenol 2004; 183(5):1479–1486.

22. Xu D, Kerwin WS, Saam T, Ferguson M, Yuan C. CASCADE: computer aided system for cardiovascular disease evaluation [abstr]. In: Proceedings of the Twelfth Meeting of the International Society for Magnetic Resonance in Medicine. Berkeley, Calif: International Society for Magnetic Resonance in Medicine, 2004; 1922.
23. Constantinides CD, Atalar E, McVeigh ER. Signal-to-noise measurements in magnitude images from NMR phased arrays. Magn Reson Med 1997;38(5):852–857.
24. Varghese A, Crowe LA, Mohiaddin RH, et al. Interstudy reproducibility of three-dimensional volume-selective fast spin echo magnetic resonance for quantifying carotid artery wall volume. J Magn Reson Imaging 2005;21(2):187–191.
25. Yuan C, Kerwin WS, Ferguson MS, et al. Contrast-enhanced high resolution MRI for atherosclerotic carotid artery tissue characterization. J Magn Reson Imaging 2002; 15(1):62–67.
26. Kolodgie FD, Gold HK, Burke AP, et al. Intraplaque hemorrhage and progression of coronary atheroma. N Engl J Med 2003; 349(24):2316–2325.
27. Takaya N, Yuan C, Chu B, et al. Association between carotid plaque characteristics and subsequent ischemic cerebrovascular events: a prospective assessment with MRI—initial results. Stroke 2006;37(3):818–823.
28. Virmani R, Kolodgie FD, Burke AP, et al. Atherosclerotic plaque progression and vulnerability to rupture: angiogenesis as a source of intraplaque hemorrhage. Arterioscler Thromb Vasc Biol 2005;25(10):2054–2061.
29. Allkemper T, Schwindt W, Maintz D, Heindel W, Tombach B. Sensitivity of T2-weighted FSE sequences towards physiological iron depositions in normal brains at 1.5 and 3.0 T. Eur Radiol 2004;14(6):1000–1004.